https://doi.org/10.1016/j.jnoncrysol.2018.07.071

Investigating relaxation of glassy materials based on natural vibration of beam: a comparative study of Borosilicate and chalcogenide glasses

Jianbiao Wang, Haihui Ruan*, Xu Wang, Jianquan Wan

Department of Mechanical Engineering, The Hong Kong Polytechnic University, Hung Hom, Kowloon, Hong Kong, China

Abstract.

The present work investigates the validity of using the frequency and decay rate of free-free beam vibration, which are measured by the impulse excitation technique (IET), to characterize the viscoelastic properties of glass in the temperature range of glass transition. Based first on the classical Burgers model, we show that the temperature-dependent flow viscosity of borosilicate glass, calculated from the measured frequency and amplitude decay rate of the flexural vibration, agrees very well with the existing data. While for chalcogenide glass, the same calculation approach does not render the similar agreement, and the reason probably lies in non-exponential effects. To comprehend the IET data in the temperature range of glass transition, we propose a simplified theoretical framework for describing the transition from the solid-like to liquid-like viscoelastic behavior and discuss the cause of difference of the rheology behaviors of these two types of glass based on the formulation of non-exponential relaxation.

Keywords: Viscosity, Young's Modulus, Optical Glass, Chalcogenide, Non-exponential relaxation, DMA

* Corresponding author Tel.: + 852 2766 6648, Fax: +852 2365 4703, E-mail address: haihui.ruan@polyu.edu.hk

Investigating relaxation of glassy materials based on natural vibration of beam: a comparative study of Borosilicate and chalcogenide glasses

Jianbiao Wang, Haihui Ruan*, Xu Wang, Jianquan Wan
Department of Mechanical Engineering, The Hong Kong Polytechnic University, Hung Hom, Kowloon, Hong Kong, China

Abstract.
The present work investigates the validity of using the frequency and decay rate of free-free beam vibration, which are measured by the impulse excitation technique (IET), to characterize the viscoelastic properties of glass in the temperature range of glass transition. Based first on the classical Burgers model, we show that the temperature-dependent flow viscosity of borosilicate glass, calculated from the measured frequency and amplitude decay rate of the flexural vibration, agrees very well with the existing data. While for chalcogenide glass, the same calculation approach does not render the similar agreement, and the reason probably lies in non-exponential effects. To comprehend the IET data in the temperature range of glass transition, we propose a simplified theoretical framework for describing the transition from the solid-like to liquid-like viscoelastic behavior and discuss the cause of difference of the rheology behaviors of these two types of glass based on the formulation of non-exponential relaxation.

Keywords: Viscosity, Young's Modulus, Optical Glass, Chalcogenide, Non-exponential relaxation, DMA

1. Introduction

Although glasses with constituents ranging from inorganic minerals and polymers to metals [1] have been extensively used in the modern world [2], the physical concept of glass transition remains a significant challenge in fundamental research [3]. The disordered atomic arrangement makes it difficult to understand physical properties based merely on microstructures and structural relaxation, leading to intricate variations in physical properties with temperature and time [4-6], which produces difficulty in predicting these properties following a certain thermal history.

Though numerous theories have been proposed to understand the nature of glass[3], the

* Corresponding author Tel.: + 852 2766 6648, Fax: +852 2365 4703, E-mail address: haihui.ruan@polyu.edu.hk

experimental characterization of glass transition is mainly based on the remarkable difference between the solid-like and liquid-like behaviors and their markedly different temperature dependence. An inflection point can be identified at the temperature-property curve, and defined as the glass transition point, T_g. Glass transition has been investigated by monitoring the temperature dependences of volume [7], enthalpy [8], refractive index [9], viscosity [10, 11], elastic modulus [12, 13] or other macroscopic properties [14]. It is not always possible to measure a physical property *in situ* in a continuous heating or cooling process. For example, the measurement of the refractive index, which is crucial for optical glasses, can only be carried out at room temperature based on quenched specimens [9]; for viscosity measurement,, different technologies must be employed in varying ranges: the rotation viscometer is used for low-viscosity measurement ($\eta < 10^8$ Pa·s), the beam bending, fiber elongation, bar torsion, and penetration methods are applied for the high-viscosity range ($\eta > 10^8$ Pa·s) [15], and the parallel plate method [16] is used for the intermediate viscosity range (10^4~10^{10} Pa·s). Kostal et al. [17] summarized 11 methods for measuring glass viscosity, which are all for isothermal measurement; that is, they are unsuitable for capturing the transient viscosity change during the heating/cooling process. Mauro et al. [18] modified the beam bending method to measure non-equilibrium viscosity which may probe the time dependence of viscosity at a constant temperature. Sellier et al. [19] proposed that the shear relaxation modulus and structural relaxation function could be measured by *in situ* monitoring variation of the glass plate thickness, which however has not been experimentally validated. In the past, differential scanning calorimetry (DSC) and dilatometry have been the most frequently adopted *in situ* methods for characterizing glass transition, and monitor changes in enthalpy and volume, respectively, during a continuous heating/cooling process [6]. Recently, the measurement of elastic modulus becomes another *in situ* method, which has been applied in studying different kinds of glasses [12, 13, 20].

Using the change in elastic modulus with temperature may be advantageous for studying glass transition, because: (i) the elastic modulus changes far more significantly than enthalpy and volume at a temperature near T_g, and (ii) the elastic modulus can be determined almost instantaneously (at very high frequency) using photoacoustic techniques[21] or more cost-effectively the impulse excited technique (IET) [22]. The elastic modulus obtained from an IET experiment is very weakly dependent on the vibration frequency, which can be considered as the instantaneous modulus, and therefore has been used to determine the glass transition point of various glasses [20] . Recently, Liu et al. [12] has further used IET to characterize the time-temperature dependence of the Young's modulus and parameterize the Tool-Narayanaswamy-Moynihan parameters.

In addition to the elastic modulus, the exponential decay rate of the flexural vibration, hereafter called decay rate for shorthand, can also be determined in IET experiments. The decay rate,

generally determined after Fourier analysis of the high frequency IET data (10^3 ~ 10^4 Hz), is equivalent to the logarithmic decrement of amplitude determined in the conventional low-frequency torsion pendulum method [23] and can also be used to understand dynamic behavior of materials [24]. The temperature dependence of the decay rate may peak at some temperatures, which renders some structural information [25] or indicates phase transformation [26]. It was also shown that after glass transition occurs, the decay rate will surge owing to the quick reduction of viscosity[13]. However, the quantitative relation between decay rate and stress relaxation is still not clear, owing partly to the rather large scattering of decay rate data in their work and, more fundamentally, the lack of a proper viscoelastic model.

In this work, we make further use IET for studying relaxations in glasses, and focus on the information that can be extracted from the decay rate. In Section 2 we report the experimental results of modulus and decay rate of typical borosilicate and chalcogenide glasses for optical application. In Section 3, the applicability of the classical Burgers model is first examined to check whether the correct flow viscosity can be determined from the decay rate. In Section 4 a theoretical framework is developed to describe the transition from the solid-like to liquid-like viscoelastic behavior and the non-exponential effects are discussed. All the remarks are concluded in Section 5.

2. Experiments and results

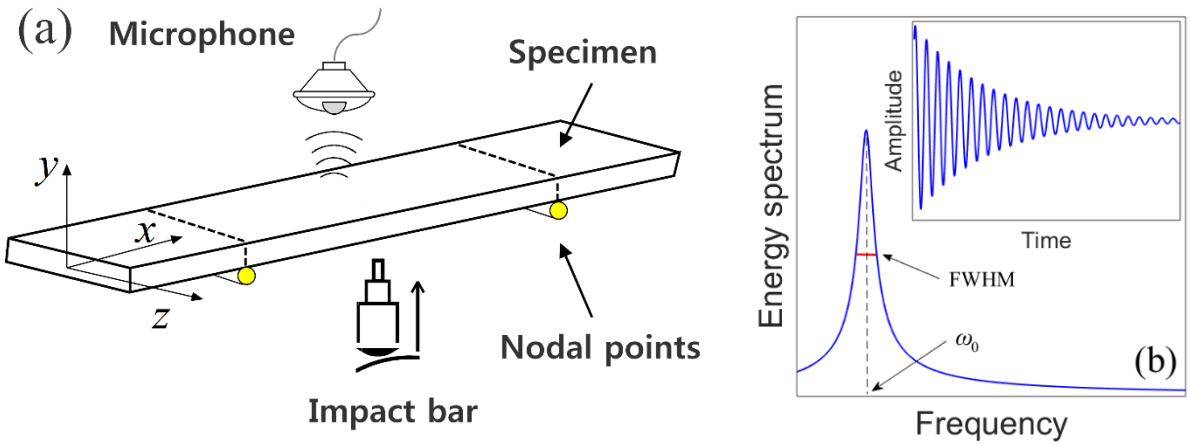

Fig. 1 Schematics of IET: (a) the setup of impulse excitation technique, and (b) the typical acoustic signal and its energy spectrum.

Fig. 1(a) displays the schematics of the IET experiment. Based on the Euler-Bernoulli beam theory, two motionless points (x = 0.224, 0.776L, where L is the beam length) exist in the first-order flexible vibration mode of an elastic free-free beam. These two points, named nodal points in Fig. 1(a), are located where the beam is hung with thin metal wires, approximately rendering the free-free beam boundary condition. Once the impact bar strikes the specimen, a damped acoustic signal will be recorded owing to the beam vibration (inset of Fig. 1(b)), which can be converted by

Fourier transform to the energy spectrum shown in Fig. 1(b). For a damped system vibrating at the angular frequency ω_d in the form of $y(t) \propto \exp(-\beta t + \mathrm{i}\omega_d t)$ with β, i, t being the decay rate, imaginary unit, and time, respectively, the peak center of the Fourier strength is considered as natural frequency ω_0 ($\omega_0^2 = \omega_d^2 + \beta^2$) and the half width at half maximum (HWHM) of the peak is considered as β. Based on the Euler-Bernoulli beam theory, the natural frequency of a pure elastic free-free beam is expressed as:

$$\omega_E = \sqrt{\lambda_n^4 E_0 I_z / (\rho L^4)}, \quad (1)$$

Where E_0, I_Z, and ρ are the Young's modulus, second moment of area, and linear density, respectively; λ_n is the modal parameter satisfying $\cos\lambda_n \cosh\lambda_n = 1$. For the first-order flexible vibration mode of a free-free beam, $\lambda_1 = 4.73$. Based on the theory of one-DOF vibration, the Fourier transform energy spectrum will peak at the frequency ω_0 and the decay rate β is approximately the half width at half maximum (HWHM) of the peak [27], as illustrated in Fig. 1(b). In the case where β is significantly smaller than ω_0 for a solid, $\omega_d \cong \omega_0 \cong \omega_E$ is generally assumed in practice. This notion, namely that the frequency at the energy spectrum peak is approximately the pure elastic beam natural frequency, is adopted in IET in order to determine the natural frequency of the beam and decay rate, which are converted into Young's modulus using Eq. (1). In case that the beam is too short or too thick, a correction factor [28] should be multiplied by Young's modulus calculated from Eq. (1), which is based on the Timoshenko beam theory [29].

Table 1 Dimensions and glass transition temperatures

Glass	Size / mm^3 (±0.01mm)	Mass / g (±0.1mg)	T_g (Viscosity)	T_g (Dilatometry)	T_g (Young's modulus)
L-BSL7	40.1×10.1×1.52	1.4644	488 °C(AP)	498 °C	484 °C (±1°C)
L-BAL42	40.08×7.98×1.97	1.9471	494 °C(AP)	506 °C	497 °C (±1°C)
IRG202	40.03×8.02×2.44	3.4572	288°C[13]	282°C	280°C (±1°C)
IRG206	40.07×8.02×2.45	3.6610	182°C[30]	180°C	177°C (±1°C)

In the experiment, we used the IET system HT1600 from IMCE, Belgium. All the units shown in Fig. 1(a) are installed in a closed furnace for studying the temperature dependence. Four types of glasses listed in Table 1 are measured in the present work, of which two are borosilicate glasses, L-BSL7 (SiO2(69.13)-B2O3(10.75)-Na2O(10.40)-K2O(6.29), wt.%) [31] and L-BAL42

(SiO_2(40-50)- BaO(20-30)-B_2O_3(2-10)-Al_2O_3(2-10)-ZnO(2-10)-Others, wt.%) [32] from OHARA Corporation; and the others are chalcogenide glasses, IRG202($Ge_{22}Se_{58}As_{20}$, mol%) and IRG206($Se_{60}As_{40}$, mol%) from Hubei New Hua-Guang Information Materials Co., Ltd. In the measurement, nitrogen gas is purged into the furnace to protect the sample from oxidation (especially for the chalcogenides). The experimental errors could arise from dimensional (±0.01 mm) and weight (±0.1mg) measurements as well as the temperature measurement (± 0.5 °C). Considering these effects, the Young's modulus determined from Eq. (1) could deviate from the actual magnitude within about ± 2 %. In addition, the measurement of decay rate is affected by the condition of support, which will be discussed later in the last of Section 3.1.

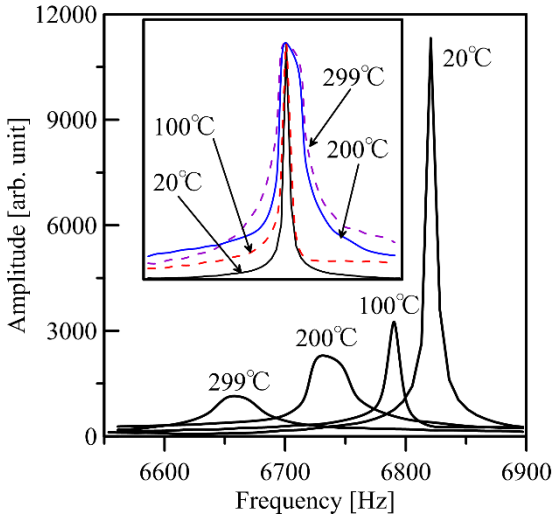

Fig. 2 Energy spectrums of the acoustic signal at different temperatures for L-BAL42

Fig. 2 displays the energy spectra of the acoustic signal at different temperatures from the L-BAL42 measurements, which illustrates that the peak position shifts to the left with increasing temperature, indicating that the modulus decreases with increasing temperature. The height of the peak reduces with temperature increase, which is owing to the increase of the decay rate. In the inset of Fig. 2, the spectra are normalized by the height and frequency of the respective maxima, indicating that the peak becomes more obtuse and the HWHM increases with the temperate rise, thereby further demonstrating the increase in decay rate. Using these clear-cut signals, we can obtain high-quality modulus and decay rate data for a glass specimen.

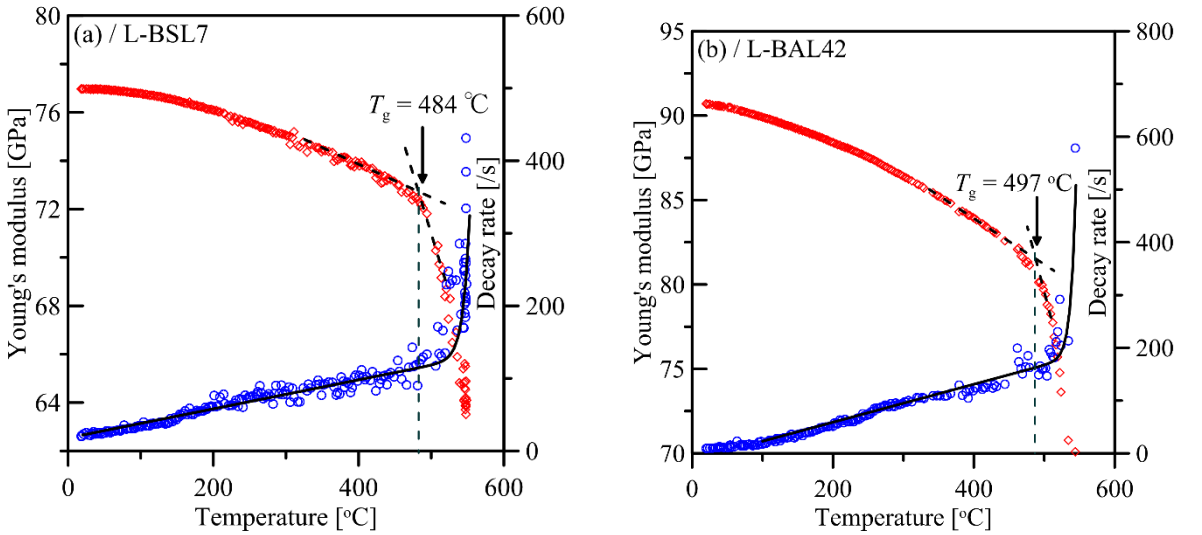

Fig.3 Variations in Young's modulus and decay rate with temperature for borosilicate glasses: (a) L-BSL7 and (b) L-BAL42. The red rhombuses and blue circles indicate Young's modulus and decay rate respectively. The relative error in determining Young's is ±2.14%.

The variations in the Young's modulus E and decay rate β of glass L-BSL7 are illustrated in Fig. 3(a). Along the Young's modulus decline with temperature, a distinct change in the decreasing rate can be identified at approximately 484°C. This temperature can be regarded as the glass transition point determined from the modulus variation. It should be noted that this temperature is approximately 14°C lower than the T_g determined by dilatometry (498°C), according to data provided by the manufacturer. Although the glass transition point T_g can be measured by various methods, it should be noted that the consensus on the definition of T_g is based on the particular magnitude of viscosity. Angell et al. [10, 11, 33] suggested that the flow viscosity η is 10^{12} Pa·s at the glass transition temperature, which hereafter is referred as $T_{g,v}$. In the glass industry, the Annealing Point (AP) is generally measured, at which the viscosity could be slightly larger than 10^{12} Pa·s (typical magnitude is $10^{12.2}$ Pa·s). Since AP is very close to $T_{g,v}$, it is directly used here to compare with other T_g measurement. The AP of L-BSL7 is 488°C, only 4 °C higher than the T_g determined based on modulus variation. This result demonstrates that measuring the modulus change is also an effective approach to investigating glass transition. Fig. 3(b) illustrates the variations in Young's modulus and decay rate of the optical glass L-BAL42. The T_g determined from the modulus variation is 497°C, which also agrees strongly with the $T_{g,v}$ of L-BAL42 (494°C, AP).

The decay rate data fluctuate far more significantly than the modulus data. Therefore, we fit these with the equation:

$$\beta = p_1 \exp\left(T/p_2\right) + p_3 + p_4 T\,, \tag{2}$$

where p_1~p_4 are fitting parameters that are listed in Table 2. This equation consists of the linear and exponential functions of temperature. It is noted that the low-temperature (below T_g) variation of decay rate is essentially linear, as shown in Fig. 3. Therefore, it is expected that the exponential term in Eq. (4) should be caused by the swift decrease of flow viscosity when the temperature is higher than I_g. In Fig. 3, a sharp increase in the decay rate can be observed. Intuitively, it would be expected that such a drastic change in decay rate occurs near T_g; however, this is not the case, as indicated in Fig. 3(a) and (b) by the vertical dashed line. In Fig. 3, the apparent sharp increase in decay rate occurs at a temperature that is at least 10°C higher than the T_g determined from the modulus variation. This deviation can be understood based on the Maxwell model provided in section 3.1. Consider the Maxwell flow viscosity in the range of 10^{10} ~ 10^{12} Pa·s. The decay rate contributed by it, given by $\beta = E/2\eta_M$ (where η_M is the flow viscosity), is within the range of 0.01 ~ 1 s^{-1}, which remains very small compared other damping effects (for example, Kelvin damping of the material and damping due to suspension wires).

Table 2 The parameters of decay rate in Eq. (2)

Eq. (4)	p_1 / s^{-1}	p_2 / °C	p_3 / s^{-1}	p_4 /(s °C)$^{-1}$
L-BSL7	1.0E-25	8.8	18	0.2
L-BAL42	5.0E-32	7	-13	0.36
IRG202	7.4E-5	24.05	2.07	0.0484
IRG206	1.58E-7	10.26	-0.55	0.1194

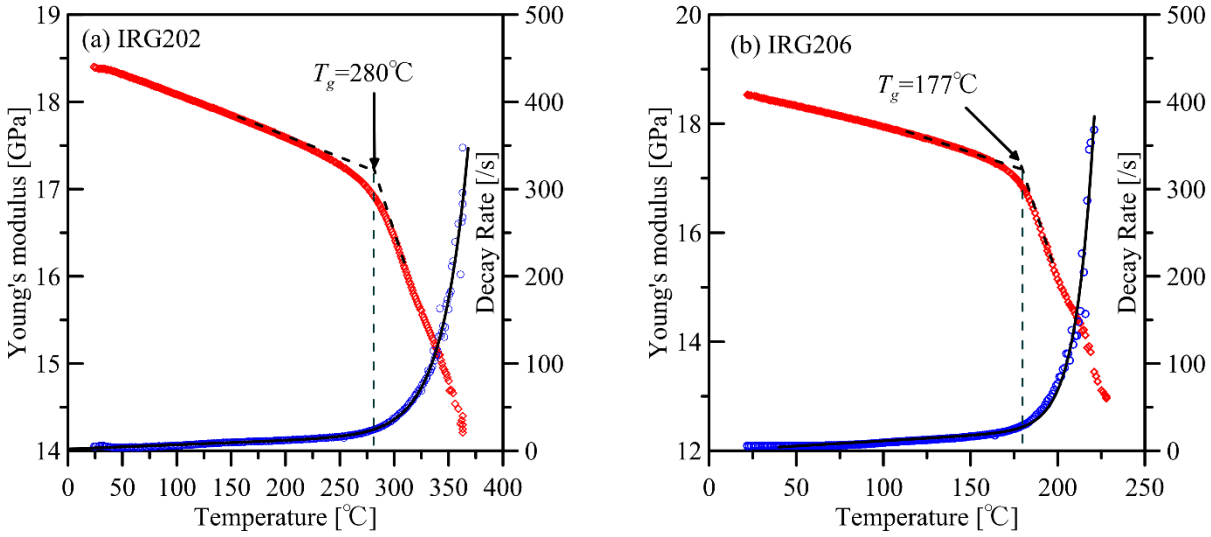

Fig.4 Variations of Young's modulus and decay rate with temperature for chalcogenide glass: a) IRG202 and b) IRG206. The red rhombuses and blue circles indicate Young's modulus and decay rate respectively. The relative error in determining Young's is ±1.46%.

The measured results for chalcogenide glasses are plotted in Fig. 4. The variations in Young's modulus of the chalcogenide glass resemble those of borosilicate glass, and the glass transition points are determined as 280°C and 177°C for IRG202 and IRG206, respectively. As opposed to the borosilicate glass cases, these two temperatures are very close to the T_g measured by dilatometry, namely 282°C and 180°C for IRG202 and IRG206, respectively. The same experiment on IRG202 was conducted by Bourhis et al. [13], who demonstrated that the T_g measured by Young's modulus was between 270~280°C, consistently with our measurement. It should be noted that Bourhis et al. [13] used silver paint to protect the sample from oxidation (whereas we simply purge nitrogen), which may affect the modulus measurement, leading to a slightly different T_g. The glass transition temperatures of the four glasses determined from the variations in modulus, viscosity, and volume expansion are summarized in Table 1. For borosilicate glasses, the T_g determined from the modulus variation is consistent with $T_{g,v}$. In contrast, the $T_{g,v}$ of either chalcogenide is higher than the T_g measured by IET and dilatometry.

The decay rate variations of the two chalcogenide glasses also differ from those of the two borosilicate glasses. It is surprising that the fluctuations in the decay rate data of chalcogenide glasses are significantly smaller than those of borosilicate glasses, as illustrated in both Figs. 4(a) and (b), the transition from the slow and linear increase to the precipitous decay rate rise is far less abrupt than that of borosilicate glasses, and the transition occurs almost exactly at the T_g, as indicated by the vertical dashed lines in Figs. 4(a) and (b). The decay rate is also fitted by Eq. (2) and the parameters are listed in Table 2.

3. Analyses: The relation between viscosity and decay rate

3.1 Vibrations of a viscoelastic beam with free-free ends

In this study, we attempt to use the vibration frequency and decay rate from IET experiments to understand the relaxation of glassy materials. Therefore, the relations between the measured variables and physical properties of the specimens are required. Numerous studies have been conducted on the vibration of a viscoelastic beam, as summarized by Adhikari [27]; however, most of them can only be solved with certain viscoelastic models. In this paper, we introduce a general framework for any viscoelastic models, for smoothing the following discussion. The issue can be started from a general dynamic stress-strain relation, expressed as:

$$\sigma(t) = \int_0^t E_0 R(t-\xi)\frac{\mathrm{d}\varepsilon}{\mathrm{d}\xi}\mathrm{d}\xi, \tag{3}$$

where σ and ε are the time-dependent normal stress and strain along the axial direction of the beam, and $R(t)$ is the relaxation (or memory) function of time t. Based on the Euler-Bernoulli beam theory, the bending moment is

$$M = \int_A \sigma y \, \mathrm{d}A, \tag{4}$$

where A is the beam cross-section area, and y is the coordinate of a point at the cross-section from the neutral axis and along the deflection direction (see Fig. 1(a)). Allowing $w(x, t)$ to be the beam deflection at the axial coordinate x and time t, the governing equation of vibration of the Euler-Bernoulli beam is:

$$\frac{\partial^2 M}{\partial x^2} + \rho \frac{\partial^2 w}{\partial t^2} = F(x,t), \tag{5}$$

where $F(x,t)$ is the external force. Using the relationship $\varepsilon = y\dfrac{\partial^2 w}{\partial x^2}$, based on the plane section assumption, Laplace transforms of Eqs. (4~6) are given as:

$$\begin{cases} \hat{\sigma} = H(s)\hat{\varepsilon} + f \\ \hat{M} = \dfrac{\partial^2 \hat{w}}{\partial x^2} H(s) I_z + g \\ \dfrac{\partial^2 \hat{M}}{\partial x^2} + \rho s^2 \hat{w} = \rho h + \hat{F}(x,s) \end{cases}, \tag{8~10}$$

where the overhead "^" represents the corresponding variable after Laplace transformation, $H(s) = E_0 \hat{R}(s) s$ is the generalized Young's modulus in the Laplace domain, s is the Laplace variable, $f = sE_0 \hat{R}(s) \cdot \varepsilon|_{t=0}$, $g = \int_A y f \, \mathrm{d}A$, and $h = s\,w|_{t=0} + (\partial w/\partial t)|_{t=0}$ are all due to initial beam deflection and deflection velocity.

Considering the case in which the initial deflection and velocity are both zero and the beam is excited by an external impulse force $F(x,t) = I_p \delta(x - L/2)\delta(t)$ at the middle span, the initial conditions can be expressed as follows:

$$\begin{cases} \varepsilon|_{t=0} = w|_{t=0} = (\partial w/\partial t)|_{t=0} = 0 \\ \hat{F}(x,s) = I_p \delta(x - L/2) \end{cases}. \tag{9}$$

Therefore, $f = g = h = 0$ and Eq. (10) is recast after substituting Eq. (9) into Eqs. (8~10) as:

$$H(s) I_z \frac{\partial^4 \hat{w}}{\partial x^4} + \rho s^2 \frac{\partial^2 \hat{w}}{\partial x^2} = I_p \delta(x - L/2). \tag{10}$$

Now, we consider the modal response and assume that

$$\hat{w}(x,s)=\sum_{m=1}^{\infty}X_m(x)\Gamma_m(s), \tag{11}$$

where $X_m(x)=C_m\left\{\cos(\lambda_m x/L)+\mathrm{ch}(\lambda_m x/L)-p\left[\sin(\lambda_m x/L)+\mathrm{sh}(\lambda_m x/L)\right]\right\}$ are the orthogonal modal function of the free-free beam, $p=\dfrac{\cosh\lambda_m-\cos\lambda_m}{\sin\lambda_m-\sinh\lambda_m}$, C_n is the normalization factor letting $\int_0^L X_n^2(x)\mathrm{d}x=1$, and $\Gamma_m(s)$ is the undetermined response function. Substituting Eq. (11) into Eq. (10) leads to:

$$\sum_{m=1}^{\infty}\left[\frac{\partial^4 X_m(x)}{\partial x^4}\Gamma_m(s)+\frac{\rho s^2}{H(s)I_z}X_m(x)\Gamma_m(s)\right]=\frac{I_p\delta(x-L/2)}{H(s)I_z}. \tag{12}$$

Using the orthogonality and normality of $X_m(x)$, $X_n(x)$ can be multiplied with both sides of Eq. (12) and these can be integrated with respect to x, resulting in:

$$\Gamma_n(s)=\frac{I_p X_n(L/2)}{H(s)I_z(\lambda_n/L)^4+\rho s^2} \tag{13}$$

It should be noted that the denominator of the right-hand side of Eq. (13) is the characteristic function of the dynamic system. Among the roots of the equation:

$$H(s)I_z(\lambda_n/L)^4+\rho s^2=0 \tag{14}$$

those with negative real parts, expressed as $s=-\beta+\mathrm{i}\omega_d$, govern the damped vibration.

The schematics of several viscoelastic models are provided in Fig. 5, for which the constitutive stress-strain relations, derived decay rates, and free vibration frequencies are listed in Table 2. Note that we denote the viscosity of the dashpot connected in parallel with a spring as η_K, which represents the Kelvin solid damping effect. Furthermore, η_M denotes the viscosity of the dashpot in series with a spring, which is the flow (or Maxwell) viscosity generally referred to in the glass research community. In the case of beam vibration, the extensional viscosity is used, which should be converted into shear viscosity for comparison with other viscosity measurements. The ratio between the shear and extensional viscosity of Newton liquids is known as the Trouton ratio, with a value of approximately 3, as proposed by Trouton [34]. This value has subsequently been validated by many experiments [35, 36]; thus, in this paper, we use the Trouton ration of 3.

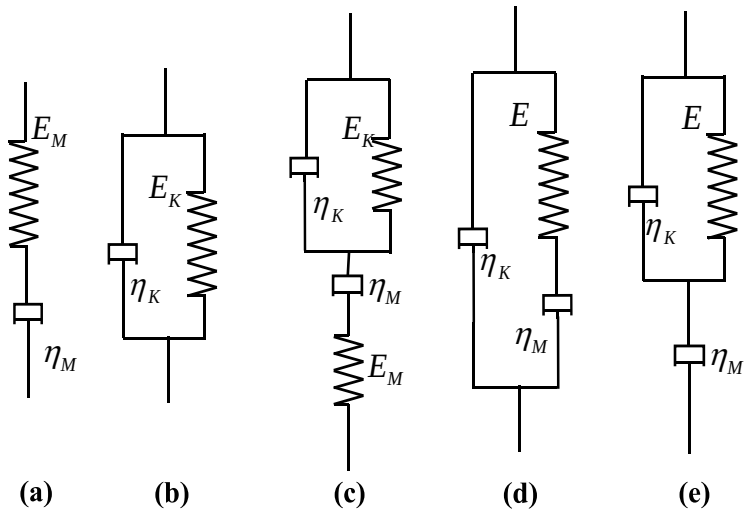

Fig. 5 Representations of viscoelastic models: (a) Maxwell model, (b) Kelvin model, (c) Burgers model, (d) Zener model [37] and (e) Jeffery model [38].

Table 3. Comparison of different viscoelastic models. ($\tau_i = \eta_i / E_i, i = K, M$)

Type	$H(s)$	β	ω_0
Maxwell	$E/\left(1+(s\tau_M)^{-1}\right)$	$1/(2\tau_M)$	ω_E
Kelvin	$(1+\tau_K s)E$	$\omega_E^2\tau_K/2$	ω_E
Zener	$\left(\frac{1}{1+(s\tau_M)^{-1}}+\tau_K s\right)E$	$\frac{1/\tau_M+\omega_E^2\tau_K}{2}$	$\omega_E\left(1+\tau_K/\tau_M\right)^{1/2}$
Jeffery	$\frac{E(\tau_K s+\tau_M\tau_K s^2)}{1+(\tau_M+\tau_K)s}$	$\frac{\tau_M^{-1}+\tau_K\omega^2}{2(1+\tau_K/\tau_M)}$	$\omega_E\left(1+\tau_K/\tau_M\right)^{-1/2}$
Burgers	$\frac{E_M(\tau_M s+\tau_M\tau_K s^2)}{1+(\tau_M+\tau_K+\chi_E\tau_M)s+\tau_K\tau_M s^2}$	$\frac{E_M+E_K-\frac{P}{U}-\frac{U}{4}}{3\eta_K}$	$\frac{\sqrt{3}}{3\eta_2}\left(\frac{P}{U}-\frac{U}{4}\right)$

NOTE: $P=\left(E_M+E_K\right)^2-3M\eta_K{}^2E_M$, $Q=2\left(E_M+E_K\right)^3+9\eta_K{}^2M\left(2E_K-E_M\right)E_M$, $M=(\frac{\lambda}{L})^4\frac{I_z}{\rho}$.

The above theoretical investigations merely consider the ideal case of a free-free beam. However, it is not possible for a beam to be completely free, which may affect the damping behaviors in IET[25]. If the supports exert a damping force on the beam, we have:

$$F(x,t)=I_p\delta(x-L/2)-c\frac{\partial w(N_1,t)}{\partial t}\delta(x-N_1)-c\frac{\partial w(N_2,t)}{\partial t}\delta(x-N_2) \tag{15}$$

where c is the damping coefficient, and N_1 and N_2 are the support positions. Thus, the response function is recast as:

$$\Gamma_n(s)=\frac{I_p X_n(L/2)/\varphi_n}{H(s)I_z\left(\lambda_n/L\right)^4+\rho s^2+sQ}, \tag{16}$$

where $Q=\frac{c}{\varphi_n}\left[X_n(N_1)\sum_{m=1}^{\infty}X_m(N_1)+X_n(N_2)\sum_{m=1}^{\infty}X_m(N_2)\right]$, and $\varphi_n=\int_0^L X_n(x)X_n(x)\mathrm{d}x$. It is learned from Eq. (13) that when N_1 and N_2 are located directly on the two fixed points, $X_1(N_1) = X_2(N_2) = 0$, which results in $Q = 0$, and the supported points have no effect on the first-order vibration as required. However, it is barely possible to place the supporting wires exactly on the two nodes; therefore, the effects of support wires are involved. Based on the models involving the Kelvin part, which has the term $s\eta_K$ in $H(s)$, the effects of support provided by sQ will be indistinguishable from the contribution of the term $s\eta_K I_z(\lambda/L)^4$.

3.2 Flow viscosity of borosilicate glass based on Burgers Model

It is well known that the decay rate results from the external and internal dissipation mechanisms [13], which can be modeled as a viscous effect. However, the conversion from the measured decay rate to the flow viscosity of glassy materials is rarely reported in the available literature. A possible reason for this is that the fundamental models, namely the Maxwell (Fig. 5(a)) and Kelvin (Fig. 5(b)) models, cannot be directly applied in order to describe the full range of temperature and time dependence, and those complex models are difficult to use owing to some undetermined fitting parameters. Scherer [39] suggested that the simplest viscoelastic model for glass is the Burgers model, namely a series combination of a Maxwell and Kelvin unit, as illustrated in Fig. 5(c). In studies on the stress relaxation or creep behavior of borosilicate glasses, the Burgers model provides an effective description of experimental results [40-42]. However, four undetermined parameters exist in the Burgers model, while we have only two measured variables, namely frequency and decay rate, in the IET experiment. Thus, additional assumptions are necessary so that the glass flow viscosity can be assessed from the IET measurements. Fortunately, certain characteristics of the Burgers model can aid in determining the flow viscosity η_M from the decay rate β.

When the Maxwell viscosity $\eta_M \to \infty$ and Kelvin $\eta_K \to 0$, the Burgers model degenerates to pure elastic cases, and the effective modulus is:

$$E_B=\frac{E_M E_K}{E_M+E_K}. \tag{17}$$

where E_M and E_K are the moduli of the Maxwell and Kelvin units, respectively. When the damping or viscous effect is negligible, the modulus measured by IET should be the effective modulus E_B.

When the temperature is low, $\eta_M \to \infty$ and the Maxwell viscosity effect vanishes. Thus, the decay rate β is only contributed by the Kelvin viscosity; that is:

$$\beta_K = \beta\left(\eta_M \to \infty\right). \tag{18}$$

It is determined that β_K is the function of the modulus ratio $\chi_E = E_M / E_K$, but is not dependent on the magnitude of either modulus, as exemplified in Fig. 6(a). Moreover, from Fig. 6(b), it can be determined that β_K is proportional to the magnitude of η_K if χ_E is fixed.

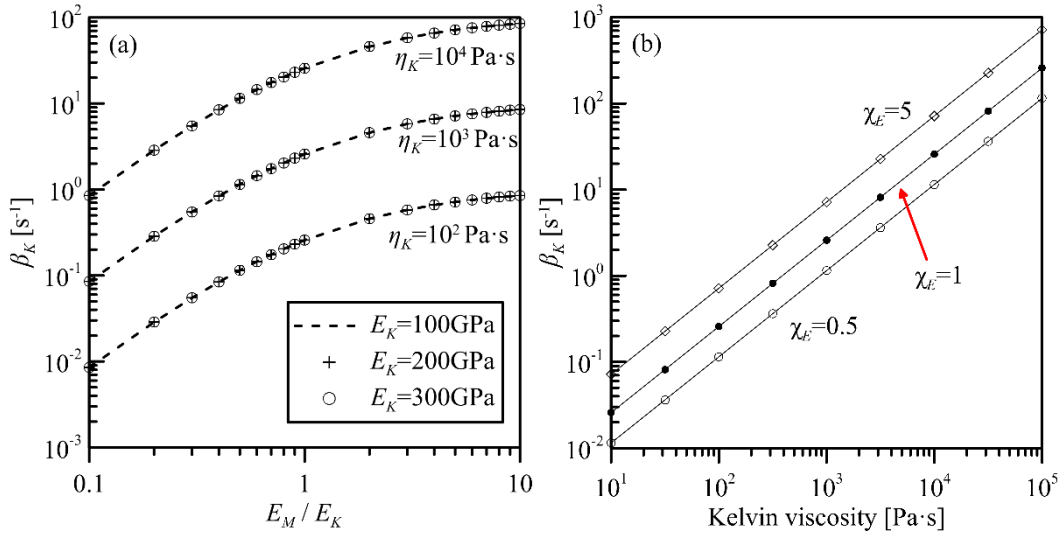

Fig. 6 Variations of decay rate on (a) modulus ratio and (b) Kelvin viscosity using specimen L-BAL42.

In the case of finite η_M, $(\beta - \beta_K)$ represents the contributions from the Maxwell viscosity and the coupled effect of the Maxwell and Kelvin units. The Burgers model degenerates to the Maxwell model when $\eta_K \to 0$. Therefore, the Maxwell viscosity contribution (refer to the decay rate derived from the Maxwell model, as shown in Table 3) can be defined as:

$$\beta_M = \beta\left(\eta_K \to 0\right) = 0.5E_B / \eta_M \tag{19}$$

We then define the variable $\alpha = \left(\beta - \beta_K\right) / \beta_M$ in order to determine the coupling effect. Fig. 7 illustrates the variation of $|\alpha - 1|$ with η_M. It is found that the value of α is very close to 1 (error less than 1%) for varied with η_K and η_M, and when χ_E is within the range of 10^{-2} and 10^{2} (note: in the fitting of experiments, for example, Refs. [40, 41], χ_E is in the range of 0.1 ~ 10). Because of this weak coupling effect, the decay rate can be expressed as $\beta \cong \beta_K + \beta_M$. Furthermore, the flow viscosity can be determined as $\eta_M = 0.5E_B / \beta_M = 0.5E_B / \left(\beta - \beta_K\right)$ if the Kelvin contribution β_K is known.

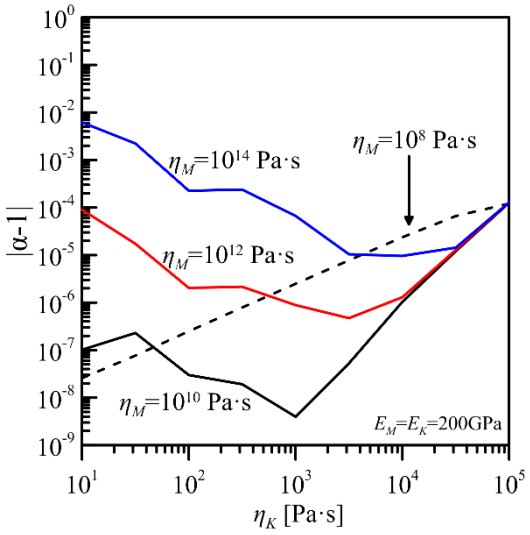

Fig. 7 $|\alpha-1|$ with varying Kelvin viscosity for L-BAL42 when η_M is near 10^{12} Pa·s.

We conceive an approach to determine the Kelvin viscosity variation with temperature. At a low temperature, the atomic system vibrates in the potential well, while at a high temperature, the system can jump out of the well to a new configuration [39]. The former situation corresponds to the Kelvin model, and the latter should at least be modeled by the Maxwell model. We assume that the relation between η_K and temperature can be extrapolated to a temperature higher than T_g. Furthermore, the difference between the actual decay rate and that extrapolated from the Kelvin model should lead to the Maxwell viscosity. As the decay rate results can be fitted effectively by Eq. (4), in which the linear terms pertain to the low-temperature variation and the exponential describes the precipitous rise at a high temperature, the exponential term $p_1\exp(T/p_2)$ in Eq. (2) can be directly used to calculate the Maxwell viscosity η_M. It should be noted that Young's modulus is involved in the viscosity calculation, for which the experimental results are used directly.

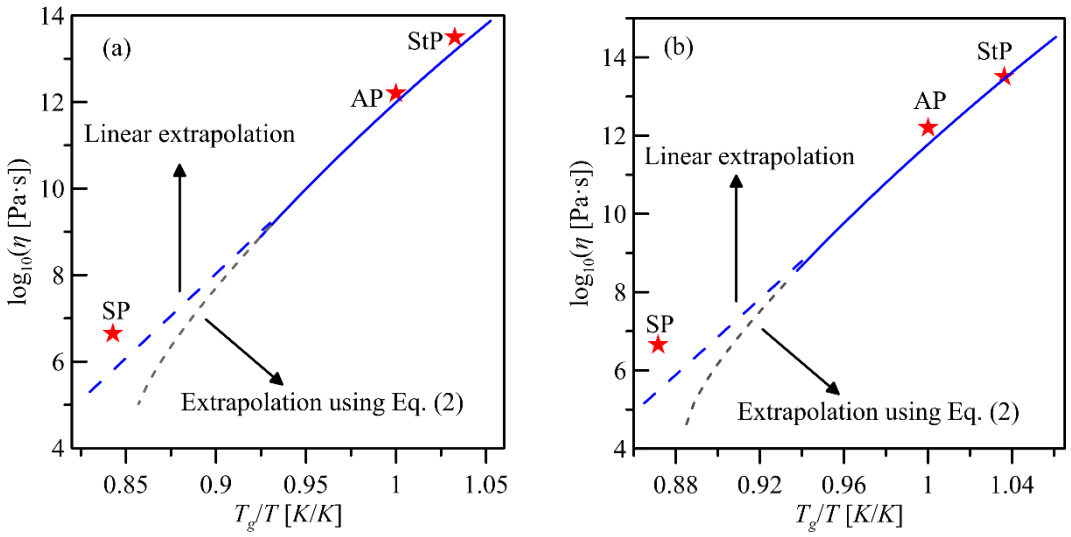

Fig. 8 Shear viscosities determined using Burgers model and plotted using the Angell plot[10] for glass (a)

L-BSL7 and (b) L-BAL42, in which the solid blue lines are calculated from decay rate based on the Burgers model.

The calculated shear viscosity is exhibited using the Angell plot, as illustrated in Figs. 8(a) and (b) for L-BSL7 and L-BAL42, respectively. The strain point (StP), $T_{g,v}$, and softening point (SP) are defined at viscosities of $10^{13.5}$, 10^{12}, and $10^{6.65}$ Pa·s, respectively, measured using a viscometer and provided by the manufacturer. The obtained viscosity curves are almost linear and well match the low-temperature ($T_{g,v}$ and StP) viscosity data provided. It should be noted that the IET data is only available at approximately 550°C (T_g /T ~ 0.93 K/K) for both glasses, at which the viscosity is approximately 10^9 Pa·s. When the viscosity is lower than this value, the acoustic signal has been too weak to obtain a clear energy spectrum peak. Therefore, we extrapolate the viscosity-temperature curve to a higher temperature. If the decay rate fitting equation is still used, the extrapolation leads to a rapid viscosity reduction and a deviation from the Vogel-Fulcher-Tamman law. In Fig. 8 (a) and (b), the fragilities can be determined to be 38 and 47 for L-BSL7 and L-BAL42, which are consistent with the measurements of Smedskjaer et al.[43]. If the results are linearly extrapolated to the higher temperature regime, the estimated viscosity would be too low as indicated by the deviation from the softening point. This indicates the non-Arrhenius character of borosilicate glasses, which can be inferred from the large fragility. Based on these observations, we conclude that the decay rate obtained from the IET experiments can effectively be used to calculate the flow viscosity borosilicate glass based on the Burgers model.

3.3 Flow viscosity of chalcogenide glass based on the Burgers model

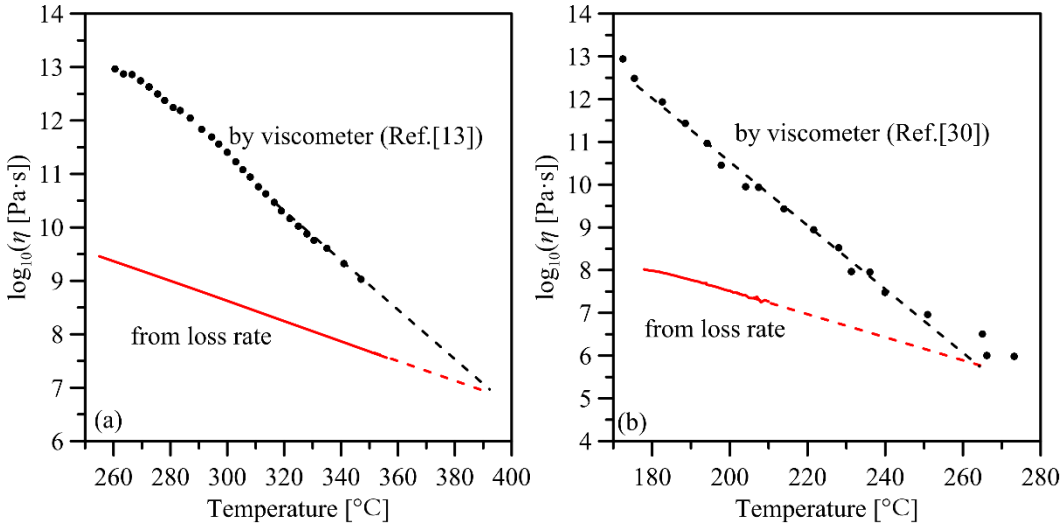

Fig. 9 Shear viscosities determined using Burgers model and viscometer for (a) IRG202 and (b) IRG206

The successful application of the Burgers model to the borosilicate glasses inspires us to

conduct a similar treatment on the decay rate data of chalcogenide glasses. The obtained viscosity is plotted in Fig. 9, in which the viscosities measured by a viscometer [13, 30] are also displayed. However, the comparison is disappointing because the viscosities obtained from the decay rates based on the Burgers model are significantly smaller than those from the viscometer, although the difference reduces with temperature. There may be two reasons for this disagreement: firstly, the linear extrapolation of the relation between the Kelvin viscosity η_K and temperature to a temperature higher than T_g may be incorrect for chalcogenide glasses; and secondly, the Burgers model may be inapplicable for describing chalcogenide glasses. In a recent study [44], it was proposed that chalcogenide glass may be non-flowing under small stress, even when the temperature is higher than the SP, indicating that the Burgers model may be invalid. A study by Bernard et al. [40] in 2007 demonstrated that, although the stress relaxation of the Te–As–Se system can be fitted by the Burgers model, the obtained parameters fail to describe the strain-recovery process. Furthermore, later work [45] illustrated that the Burgers model cannot model the relaxation in both short and long periods of Te–As–Se and Ge-Se glasses. These studies suggest that the viscoelastic behaviors of chalcogenide glass are fundamentally different from those of borosilicate glass, which needs further discussion (in Section 4.2).

4. Discussions

4.1 Simplified model for transition from solid-like to liquid-like behaviors

The above analysis raises the more fundamental question of how to select a viscoelastic model for describing viscoelastic behavior in the glass transition temperature range, and what the physical picture is if a viscoelastic model is selected. Without a clear physical picture, the fundamental difference between the borosilicate and the chalcogenide glasses is still vague. In order to answer these questions, we first establish a minimal model to describe the effects of glass transition on the stress-strain relation of a glassy material, expressed as Eq. (3).

We begin with a mosaic picture of glass transition [46], whereby a glass may be simplified into many small patches (that is, the atomic subsystem), which can spontaneously change their configuration when the temperature is elevated to the glass transition range. Assume that such a configuration change occurs within the infinitesimal time span $[\tau, \tau+\mathrm{d}\tau]$ with a probability $J\mathrm{d}\tau$, where J is the transition rate, and that such a transition leads to a total loss of memory and zero stress at the transition instant τ. We then follow the behavior of a single patch, which may or may

not change its configuration over time [0, t]. The details of these two scenarios are described as follows.

(1) The patch does not change its configuration during the time [0, t] with a probability $P(t)$. As the configuration does not change, we assume that the mechanical behavior should be solid-like, represented by the relaxation function $R_0(t)$.

(2) The patch does not change its configuration during the time [0, τ], and then changes at the instant τ. The joint probability is then $P(\tau)Jd\tau$, and the total probability of this behavior, when the instant τ runs from 0 to t, is $\int_0^t P(\tau)J\mathrm{d}\tau$. It should be noted that the patch changes its configuration at τ and can change further, multiple times, during the time span [τ, t], which depicts structural relaxation and liquid-like behavior [47]. Therefore, a new relaxation function, different from the above solid-like function $R_0(t)$, must be assumed. We assume that this relaxation function is identical to that of the entire system $R(t)$, based on the rationale that the response of a single patch over a sufficiently lengthy period (time average) should be identical to the average response of many patches (ensemble average).

The summation of the above two scenarios leads to the average stress at time t, which reads:

$$\begin{aligned}\sigma(t) &= \int_0^t E_0 R(t-\xi)\frac{\mathrm{d}\varepsilon}{\mathrm{d}\xi}\mathrm{d}\xi \\ &= P(t)\int_0^t E_0 R_0(t-\xi)\frac{\mathrm{d}\varepsilon}{\mathrm{d}\xi}\mathrm{d}\xi + \int_0^t P(\tau)\left\{\int_\tau^t E_0 R(t-\xi)\frac{\mathrm{d}\varepsilon}{\mathrm{d}\xi}\mathrm{d}\xi\right\}J\mathrm{d}\tau\end{aligned}, \tag{20}$$

The summation rule of probability requires $P(t)+\int_0^t P(\tau)J\mathrm{d}\tau = 1$, for which the solution is

$$P(t) = \exp(-Jt). \tag{21}$$

By substituting Eq. (21) into (20) and changing the integration order of ξ and τ, we obtain:

$$\begin{aligned}\int_0^t R(t-\xi)\frac{\mathrm{d}\varepsilon}{\mathrm{d}\xi}d\xi &= e^{-Jt}\int_0^t R_0(t-\xi)\frac{\mathrm{d}\varepsilon}{\mathrm{d}\xi}d\xi + \int_0^t\left\{\int_0^\xi R(t-t')\frac{\mathrm{d}\varepsilon}{\mathrm{d}\xi}Je^{-J\tau}d\tau\right\}d\xi \\ &= \int_0^t R_0(t-\xi)e^{-Jt}\frac{\mathrm{d}\varepsilon}{\mathrm{d}\xi}d\xi - \int_0^t R(t-\xi)\left(e^{-J\xi}-1\right)\frac{\mathrm{d}\varepsilon}{\mathrm{d}\xi}d\xi\end{aligned}, \tag{22}$$

which can be further simplified as:

$$\int_0^t R_0(t-\xi)e^{-Jt}\frac{\mathrm{d}\varepsilon}{\mathrm{d}\xi}d\xi = \int_0^t R(t-\xi)e^{-J\xi}\frac{\mathrm{d}\varepsilon}{\mathrm{d}\xi}d\xi. \tag{23}$$

We then apply Laplace transformation to Eq.(23), rendering:

$$\hat{R}(s) = \hat{R}_0(s + J). \tag{24}$$

If the material is purely elastic before glass transition (no viscous effects), we have $R_0(t) = 1$ leading to $\hat{R}_0(s) = \hat{R}_E(s) = 1/s$. With a non-zero transition rate *J*, the relaxation function becomes

$$\hat{R}(s) = \hat{R}_E(s + J) = 1/(s + J), \tag{25}$$

which represents the Maxwell model. If the material is the Kelvin solid prior to glass transition, described by $\hat{R}_0(s) = \hat{R}_K(s) = 1/s + \tau_K$, the memory function following glass transition is:

$$\hat{R}(s) = \hat{R}_K(s + J) = 1/(s + J) + \tau_K, \tag{26}$$

which is the Zener model, as illustrated in Fig. 5(d). The solution in Table 3 demonstrates that the decay rate derived from the Zener model is the sum of those provided by the Kelvin and Maxwell models, which is identical to the above calculation derived from the Burgers model. It should be noted that no coupling term of η_K and η_M exists in the decay rate expression from the Zener model. However, with the Burgers model, these two viscous units are weakly coupled when the ratio of two elastic constants χ_E is within the range of [10^{-2}, 10^2]. Moreover, the Kelvin damping assumed in the model, manifested as the non-vanishing decay rate at a low temperature, may not arise from the material response alone. The hanging wire causes the same damping effect, which cannot be distinguished from the Kelvin damping of the materials, as analyzed in section 3.1. However, as the coupling between the Kelvin damping and flow viscosity is very weak (or vanishing based on the Zener model), the flow viscosity determined from the decay rate data is therefore sensible for borosilicate glasses.

Before closing this discussion, a brief discussion on the Jeffery model (Fig. 5(e)) which is also widely used to study slow relaxation is needed. The Jeffery model is very similar to the Zener model, containing three parameters, which can also be derived from the Burger's model when χ_E is very large. Based on the decay rate formulae provided in Table 3, The Jeffery model renders $\tau_M^{Jeffery} = (1 - 2\beta\tau_K)/(2\beta - \omega^2\tau_K)$, which is smaller than that based on the Zener model with the same β and τ_K, $\tau_M^{Zener} = 1/(2\beta - \omega^2\tau_K)$. When τ_K is small (in most cases of glass it is), the two types of relaxation time are almost the same.

4.2 Effect of non-exponential relaxation

For the chalcogenide glasses, greater consideration is required, as their relaxation behaviors are

apparently more complex than those of borosilicate glasses. In the Burgers model, the Maxwell unit, which describes an exponential relaxation, may be too simplistic to capture the relaxation behavior in chalcogenide glass, leading to the apparent disparity as illustrated in Fig. 9. Therefore, the non-exponential relaxation should be considered.

The most important feature of a non-exponential relaxation is that the loss spectrum of the corresponding linear response, expressed as $\chi(\mathrm{is}) = 1 - s\hat{R}(s)$ [48, 49] , becomes broader than that of an exponential decay. This is known as the stretching phenomenon, which may be fitted by various expressions [49]. The most widely adopted time-domain relaxation function is probably the Kohlrausch-Williams-Watts (KWW) function $R(t) = \exp\left(-(t/\tau)^{B_{KWW}}\right)$ [50], where τ is the relaxation time and B_{KWW} is the stretched exponent, which is generally smaller than one. The Laplace transform of the KWW function is nontrivial; therefore, other Laplace domain expressions of the linear response function χ(is) were proposed, which is more convenient for fitting the stretched loss spectrum. These expressions are also more convenient for studying the beam vibration in this work, as the response function Eq. (16) is also expressed in the Laplace domain. In the following, we proceed to use the Cole-Davidson (CD) [51] expression: $\chi_{CD}(\mathrm{is}) = \dfrac{1}{(1+s\tau)^{B_{CD}}}$,

where B_{CD} is also a stretched exponent. Using the least-squares method, Lindsey and Patterson [52] provided the relation between B_{CD} and B_{KWW}:

$$B_{\mathrm{KWW}} = \begin{cases} 0.970B_{\mathrm{CD}} + 0.144, & 0.2 \le B_{B_{\mathrm{CD}}} \le 0.6 \\ 0.683B_{\mathrm{CD}} + 0.316, & 0.6 \le B_{B_{\mathrm{CD}}} \le 1.0 \end{cases}, \tag{27}$$

which can then be used to convert B_{CD} into B_{KWW}.

The CD expression leads to the relaxation function[49]:

$$\hat{R}(s) = \frac{1}{s}\left(1 - \frac{1}{(1+s\tau)^{B_{CD}}}\right). \tag{28}$$

The viscosity measurement; for example, using the beam bending method for the viscosity range in this work, is conducted in the time domain. This is the process of obtaining the strain rate under a constant stress σ_0, which is expressed as

$$\frac{d\varepsilon}{dt} = \frac{\sigma_0}{\eta(t)}. \tag{29}$$

The strain rate is usually not a constant in a short time but levels off after a sufficient time, and a

steady viscosity value is then obtained. Using the Laplace transform of Eq. (3): $\hat{\sigma}(s) = E_0 sR(s)\hat{\varepsilon}(s)$, this measurement process is expressed as:

$$\lim_{t\to\infty}\frac{d\varepsilon}{dt} = \frac{\sigma_0}{\eta} = \frac{\sigma_0}{E_0}\lim_{t\to\infty}\mathcal{L}^{-1}\left(\frac{1}{s\hat{R}(s)}\right) = \frac{\sigma_0}{E_0\hat{R}(s\to 0)} \tag{30}$$

where $\mathcal{L}^{-1}$ indicates the inverse Laplace transform. The proof of the final equality is based on the identity $\lim_{t\to\infty}F(t) = \lim_{t\to\infty}\int_0^t dF/dt\,dt = \lim_{s\to 0}s\hat{F}(s)$. The viscosity based on the CD expression Eq. (28) can then be obtained as follows:

$$\eta_{vis} = E_0\hat{R}(s\to 0) = E_0\tau B_{CD}\,. \tag{31}$$

Obviously, when $B_{\mathrm{CD}} = 1$, the Maxwell expression $\eta = E_0\tau$ is recovered.

Eq. (31) represents the viscosity measured by a viscometer of a non-exponential relaxation glass. A comparison between the IET and viscometer measurement can finally be established based on Eqs. (28) and (31). We firstly substitute Eq. (28) into Eq. (16) in order to obtain the response function induced by the non-exponential relaxation. For any given B_{CD} within the range of [0, 1], E_0 and τ are adjusted to match the peak center and HWHM with the experimental results. After E_0 and τ are determined, η_{vis} is calculated using Eq. (31). If the calculated η_{vis} is the same as the value from the viscometer experiment, the corresponding B_{CD} is selected. Then, using Eq. (27), B_{CD} is converted into B_{KWW}.

Fig. 10(a) and (b) illustrate the calculated viscosity variation with varying B_{CD} for IRG202 and IRG206, respectively. The calculated viscosity decreases monotonously with an increase in B_{CD}. Therefore, the viscosity measured by the viscometer will only correspond to one B_{CD} at a specific temperature. It is finally determined that the stretched exponent B_{KWW} at $T_{g,v}$ is ~0.42 for IRG202 and ~0.43 for IRG206, both being markedly smaller than one. It is noted that the fragility m is 28 for IRG202 and 41 for IRG206, based on the viscosity-temperature curves (measured by viscometer) shown in Fig. 9. With such a small magnitude of m, B_{KWW} is markedly smaller than that expected from the correlation map between the fragility and stretched exponent proposed by Böhmer et al. [53], which is labeled as "BNAP region" in Fig. 10(c). This deviation may be attributed to the short-time (much less than one second) dynamics probed by IET, which may not be captured by a stress relaxation experiment based on tensile tests [54], or to the specific chemical structures of these two chalcogenide glasses. Furthermore, we note that other studies have reported similar small B_{KWW} values for certain chalcogenide glasses, as plotted in Fig. 10(c). For example,

Gueguen et al. [45] conducted stress relaxation experiments on serval chalcogenide glasses Ge_xSe_{1-x}, and found that B_{KWW} is within the range of [0.22, 0.26], while the fragilities range from 32 to 37 [55]. Li et al. [56] found that $Ge_{22}Se_{78}$ has a fragility of 27 and also a very small B_{KWW} = 0.43, which is identical to our result. They suggested that the cause of small B_{KWW} could be the mixing effect of basic structural motifs.

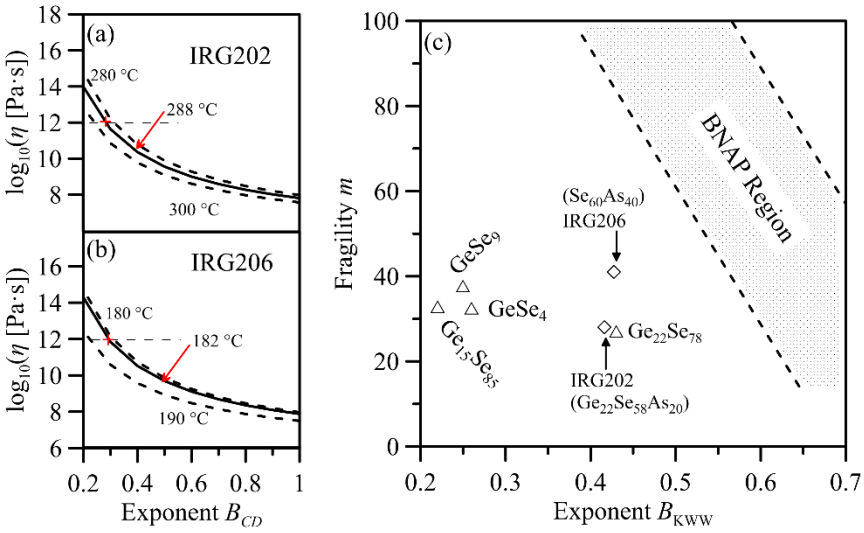

Fig. 10 The effect of stretching exponent on the calculated viscosity for (a) IRG202 and (b) IRG206 and (c) the correlation between the fragility versus stretching exponent. The data points of some chalcogenide glasses (including this work) are outside the BNAP region [53].

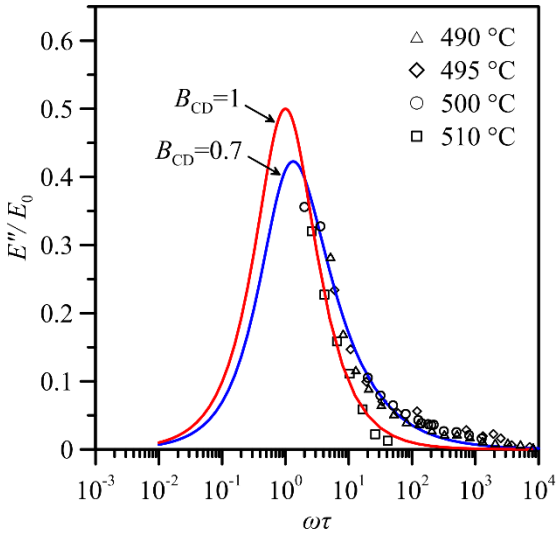

Fig. 11 Loss spectrum of L-BAL42 at the temperature of 490, 495, 500 and 510 °C. DMA data are normalized using E_0 = 82, 81, 80, 78 GPa and τ =130, 60, 20 and 10.4 s, for the four temperatures respectively.

For borosilicate glasses, it is expected that non-exponential relaxation is insignificant, which is the reason of the agreement of viscosities calculated from decay rate and measured by viscometer as shown in Fig. 8. To verify this point, DMA experiments are conducted (using Mettler Toledo

DMA1) to obtain the loss spectrum of the dynamic modulus which can be fitted with the expression of loss modulus E'' derived from the CD expression, as:

$$\frac{E''}{E_0} = \left[1+\left(\omega\tau\right)^2\right]^{-B_{\mathrm{CD}}/2} \sin\left[B_{\mathrm{CD}} \arctan\left(\omega\tau\right)\right], \tag{32}$$

where ω is the stimulated frequency. Fig.11 then shows DMA results of E''/E_0 against $\omega\tau$, in which E_0 and τ are obtained based on the IET results (i.e., from Figs. 3(b) and 8(b) respectively). The data points collapse onto the narrow region bounded by the curves of Eq. (34) with B_{CD} = 0.7 and 1. It is noted that the curve of Eq. (32) with B_{CD} = 0.7 (i.e., B_{KWW}=0.8) well fits the loss spectrum at the temperatures near T_g (490~500°C) and that the loss spectrum at the higher temperature of 510°C becomes almost unstretched (B_{CD} = 1). These results corroborate the large (close to unity) stretching exponent of the examined borosilicate glass and also indicate the consistency of IET and DMA measurements.

5. Concluding remarks

This work examines the validity of applying the IET to studying structural relaxation in glass. It is demonstrated that the temperature dependence of Young's modulus can be utilized to study the glass transition phenomenon for both borosilicate and chalcogenide glass. Furthermore, the flow viscosity of borosilicate glass can be determined from the decay rate data, based on the Burgers or Zener model; however, a more elaborate model is required for chalcogenide glass. Based on the theoretical and experimental investigations, the following remarks are made:

(1) The glass transition point determined from the modulus variation with temperature is very close to $T_{g,v}$ for the examined borosilicate glasses. However, this is not the case for the chalcogenide glasses.

(2) The flow viscosity of borosilicate glass determined from the decay rate data agrees well with the measurements using a viscometer, indicating that the Burgers or Zener model can be used, and that our approach of linear extrapolation of the Kelvin damping contribution is sensible. However, the same approach does not work for the chalcogenide glasses.

(3) A minimal model describing the transition from solid-like to liquid-like behavior is proposed, which can aid in choosing a viscoelastic model. For the borosilicate glasses, the low-temperature behavior may be purely elastic or Kelvin-Voigt, leading to a single structural relaxation time following glass transition. This is the fundamental reason that the viscosity determined from the decay rate data can match that measured by the viscometer.

(4) For chalcogenide glass, the large discrepancy in viscosities, as estimated from the decay rate of

the IET tests and measured by the viscometer, is resulted from the Burgers model. This indicates a striking non-exponential relaxation, which cannot be described by the single Maxwell unit in the Burgers model. The CD expression is then used to evaluate the effect of non-exponentiality and to estimate the stretched exponent in a KWW expression. The stretching exponent at $T_{g,v}$ is about 0.4 for both chalcogenide glasses, which is consistent with some investigations.

Acknowledgment

This work was supported by the Early Career Scheme (ECS) of the Hong Kong Research Grants Council (Grant No. 25200515, Account Code: F-PP27) and the Internal Research Funds (G-YBDH) of Hong Kong Polytechnic University. We are grateful for the support.

References

[1] J. Forrest, K. Dalnoki-Veress, J. Stevens, J. Dutcher, Effect of free surfaces on the glass transition temperature of thin polymer films, Phys. Rev. Lett., 77 (1996) 2002-2005.
[2] P.G. Debenedetti, F.H. Stillinger, Supercooled liquids and the glass transition, Nature, 410 (2001) 259-267.
[3] A. Cavagna, Supercooled liquids for pedestrians, Phys. Rep., 476 (2009) 51-124.
[4] A.Q. Tool, Relation between inelastic deformability and thermal expansion of glass in its annealing range, J. Am. Ceram. Soc., 29 (1946) 240-253.
[5] O. Narayanaswamy, A model of structural relaxation in glass, J. Am. Ceram. Soc., 54 (1971) 491-498.
[6] C.T. Moynihan, A.J. Easteal, J. Wilder, J. Tucker, Dependence of the glass transition temperature on heating and cooling rate, The journal of physical chemistry, 78 (1974) 2673-2677.
[7] G.A. Medvedev, A.B. Starry, D. Ramkrishna, J.M. Caruthers, Stochastic model for volume relaxation in glass forming materials: Local specific volume model, Macromolecules, 45 (2012) 7237-7259.
[8] M. Yang, X. Liu, H. Ruan, Y. Wu, H. Wang, Z. Lu, High thermal stability and sluggish crystallization kinetics of high-entropy bulk metallic glasses, J. Appl. Phys., 119 (2016) 245112.
[9] S. Wemple, Refractive-index behavior of amorphous semiconductors and glasses, Phys. Rev. B, 7 (1973) 3767.
[10] C.A. Angell, K.L. Ngai, G.B. McKenna, P.F. McMillan, S.W. Martin, Relaxation in glassforming liquids and amorphous solids, J. Appl. Phys., 88 (2000) 3113-3157.
[11] C.A. Angell, Formation of glasses from liquids and biopolymers, Science, 267 (1995) 1924-1935.
[12] W. Liu, H. Ruan, L. Zhang, Revealing Structural Relaxation of Optical Glass Through the Temperature Dependence of Young's Modulus, J. Am. Ceram. Soc., 97 (2014) 3475-3482.
[13] E. Le Bourhis, P. Gadaud, J.-P. Guin, N. Tournerie, X. Zhang, J. Lucas, T. Rouxel, Temperature dependence of the mechanical behaviour of a GeAsSe glass, Scripta Mater., 45 (2001) 317-323.
[14] A.M. Glass, Investigation of the electrical properties of Sr1− x Ba x Nb2O6 with special reference to pyroelectric detection, J. Appl. Phys., 40 (1969) 4699-4713.
[15] H. Kobayashi, Y. Hiki, H. Takahashi, An experimental study on the shear viscosity of solids, J. Appl. Phys., 80 (1996) 122-130.
[16] A. Gent, Theory of the parallel plate viscometer, Br. J. Appl. Phys., 11 (1960) 85.
[17] P. Koštál, J. Shánělová, J. Málek, Viscosity Measurements Applied to Chalcogenide

Glass-Forming Systems, in: J. Šesták, J.J. Mareš, P. Hubík (Eds.) Glassy, Amorphous and Nano-Crystalline Materials: Thermal Physics, Analysis, Structure and Properties, Springer Netherlands, Dordrecht, 2011, pp. 165-178.
[18] J.C. Mauro, D.C. Allan, M. Potuzak, Nonequilibrium viscosity of glass, Phys. Rev. B, 80 (2009) 094204.
[19] M. Sellier, C.E. Hann, N. Siedow, Identification of relaxation functions in glass by mean of a simple experiment, J. Am. Ceram. Soc., 90 (2007) 2980-2983.
[20] P. Mezeix, F. Célarié, P. Houizot, Y. Gueguen, F. Munoz, T. Rouxel, Elasticity and viscosity of BaOTiO2SiO2 glasses in the 0.9 to 1.2 Tg temperature interval, J. Non·Cryst. Solids, 445 (2016) 45-52.
[21] T. Hecksher, D.H. Torchinsky, C. Klieber, J.A. Johnson, J.C. Dyre, K.A. Nelson, Toward broadband mechanical spectroscopy, Proceedings of the National Academy of Sciences, (2017) 201707251.
[22] G. Roebben, B. Bollen, A. Brebels, J. Van Humbeeck, O. Van der Biest, Impulse excitation apparatus to measure resonant frequencies, elastic moduli, and internal friction at room and high temperature, Rev. Sci. Instrum., 68 (1997) 4511-4515.
[23] J.D. Ferry, Viscoelastic properties of polymers, John Wiley & Sons, 1980.
[24] I. Pereira, Overview on Determination of Elastic and Damping Properties of Different Materials using Impulse Excitation Technique, U. Porto Journal of Engineering, 3 (2017) 35-41.
[25] E. Gregorová, W. Pabst, P. Diblíková, V. Nečina, Temperature dependence of damping in silica refractories measured via the impulse excitation technique, Ceram. Int., 44 (2018) 8363-8373.
[26] G. Roebben, B. Basu, J. Vleugels, O. Van der Biest, Transformation-induced damping behaviour of Y-TZP zirconia ceramics, J. Eur. Ceram. Soc., 23 (2003) 481-489.
[27] S. Adhikari, Structural dynamic analysis with generalized damping models: analysis, John Wiley & Sons, 2013.
[28] E. ASTM, Standard test method for dynamic Young's modulus, shear modulus, and Poisson's ratio by sonic resonance, in: Annual Book of ASTM Standards, 1875.
[29] E. Goens, Über die bestimmung des elastizitätsmoduls von stäben mit hilfe von biegungsschwingungen, Annalen der Physik, 403 (1931) 649-678.
[30] A. Tverjanovich, Temperature dependence of the viscosity of chalcogenide glass-forming melts, Glass Phys. Chem, 29 (2003) 532-536.
[31] W. Liu, L. Zhang, K. Mylvaganam, Relaxation oscillation of borosilicate glasses in supercooled liquid region, Scientific reports, 7 (2017) 15872.
[32] J. Yan, T. Zhou, J. Masuda, T. Kuriyagawa, Modeling high-temperature glass molding process by coupling heat transfer and viscous deformation analysis, Precision Engineering, 33 (2009) 150-159.
[33] M.D. Ediger, C. Angell, S.R. Nagel, Supercooled liquids and glasses, The journal of physical chemistry, 100 (1996) 13200-13212.
[34] F.T. Trouton, On the coefficient of viscous traction and its relation to that of viscosity, Proceedings of the Royal Society of London. Series A, Containing Papers of a Mathematical and Physical Character, (1906) 426-440.
[35] R.B. Bird, R.C. Armstrong, O. Hassager, Dynamics of polymeric liquids. Volume 1: fluid mechanics, A Wiley-Interscience Publication, John Wiley & Sons, (1987).
[36] S. Różańska, J. Różański, M. Ochowiak, P. Mitkowski, Extensional viscosity measurements of concentrated emulsions with the use of the opposed nozzles device, Brazilian Journal of Chemical Engineering, 31 (2014) 47-55.

[37] F. Mainardi, G. Spada, Creep, relaxation and viscosity properties for basic fractional models in rheology, Eur. Phys. J. Spec. Top., 193 (2011) 133-160.
[38] P. Oswald, Rheophysics: the deformation and flow of matter, Cambridge University Press, New York, 2009.
[39] G.W. Scherer, Relaxation in glass and composites, (1986).
[40] C. Bernard, G. Delaizir, J.-C. Sangleboeuf, V. Keryvin, P. Lucas, B. Bureau, X.-H. Zhang, T. Rouxel, Room temperature viscosity and delayed elasticity in infrared glass fiber, J. Eur. Ceram. Soc., 27 (2007) 3253-3259.
[41] C. Perez, V. Alvarez, A. Vazquez, Creep behaviour of layered silicate/starch–polycaprolactone blends nanocomposites, Mater. Sci. Eng., A, 480 (2008) 259-265.
[42] T. Zhou, J. Yan, J. Masuda, T. Kuriyagawa, Investigation on the viscoelasticity of optical glass in ultraprecision lens molding process, J. Mater. Process. Technol., 209 (2009) 4484-4489.
[43] M.M. Smedskjaer, J.C. Mauro, R.E. Youngman, C.L. Hogue, M. Potuzak, Y. Yue, Topological principles of borosilicate glass chemistry, The Journal of Physical Chemistry B, 115 (2011) 12930-12946.
[44] T. Zhou, Zhou, Q., Xie, J., Liu, X., Wang, X.,, H. Ruan, Elastic‐viscoplasticity modeling of the thermo‐mechanical behavior of chalcogenide glass for aspheric lens molding, Int. J. Appl. Glass Sci., (2017).
[45] Y. Gueguen, J.-C. Sangleboeuf, V. Keryvin, T. Rouxel, E.A. King, E. Robin, G. Delaizir, B. Bureau, X.-H. Zhang, P. Lucas, Sub-Tg viscoelastic behaviour of chalcogenide glasses, anomalous viscous flow and stress relaxation, J. Ceram. Soc. Jpn., 116 (2008) 890-895.
[46] T. Kirkpatrick, D. Thirumalai, P.G. Wolynes, Scaling concepts for the dynamics of viscous liquids near an ideal glassy state, Phys. Rev. A, 40 (1989) 1045.
[47] J.C. Dyre, N.B. Olsen, T. Christensen, Local elastic expansion model for viscous-flow activation energies of glass-forming molecular liquids, Phys. Rev. B, 53 (1996) 2171.
[48] R. Kubo, Statistical-mechanical theory of irreversible processes. I. General theory and simple applications to magnetic and conduction problems, J. Phys. Soc. Jpn., 12 (1957) 570-586.
[49] W. Gotze, L. Sjogren, Relaxation processes in supercooled liquids, Rep. Prog. Phys., 55 (1992) 241.
[50] G. Williams, D.C. Watts, Non-symmetrical dielectric relaxation behaviour arising from a simple empirical decay function, Trans. Faraday Society, 66 (1970) 80-85.
[51] D.W. Davidson, R.H. Cole, Dielectric relaxation in glycerol, propylene glycol, and n‐propanol, J. Chem. Phys., 19 (1951) 1484-1490.
[52] C. Lindsey, G. Patterson, Detailed comparison of the Williams–Watts and Cole–Davidson functions, J. Chem. Phys., 73 (1980) 3348-3357.
[53] R. Böhmer, K. Ngai, C.A. Angell, D. Plazek, Nonexponential relaxations in strong and fragile glass formers, J. Chem. Phys., 99 (1993) 4201-4209.
[54] R. Böhmer, C.A. Angell, Correlations of the nonexponentiality and state dependence of mechanical relaxations with bond connectivity in Ge-As-Se supercooled liquids, Phys. Rev. B, 45 (1992) 10091.
[55] U. Senapati, A.K. Varshneya, Viscosity of chalcogenide glass-forming liquids: an anomaly in the ‘strong’and ‘fragile’classification, J. Non·Cryst. Solids, 197 (1996) 210-218.
[56] P. Li, Y. Zhang, Z. Chen, P. Gao, T. Wu, L.-M. Wang, Relaxation dynamics in the strong chalcogenide glass-former of Ge 22 Se 78, Scientific reports, 7 (2017) 40547.